ACS APPLIED ENGINEERING MATERIALS

pubs.acs.org/acsaenm

Article

Evolution of Glassy Carbon Derived from Pyrolysis of Furan Resin

Josh Kemppainen, Ivan Gallegos, Aaron S. Krieg, Jacob R. Gissinger, Kristopher E. Wise, Margaret Kowalik, Julia A. King, S. Gowtham, Adri van Duin, and Gregory M. Odegard*

Cite This: ACS Appl. Eng. Mater. 2023, 1, 2555−2566

Read Online

ACCESS | Metrics & More | Article Recommendations | Supporting Information

ABSTRACT: Glassy carbon (GC) material derived from pyrolyzed furan resin was modeled by using reactive molecular dynamics (MD) simulations. The MD polymerization simulation protocols to cure the furan resin precursor material are validated via comparison of the predicted density and Young's modulus with experimental values. The MD pyrolysis simulations protocols to pyrolyze the furan resin precursor is validated by comparison of calculated density, Young's modulus, carbon content, sp^2 carbon content, the in-plane crystallite size, out-of-plane crystallite stacking height, and interplanar crystallite spacing with experimental results from the literature for furan resin derived GC. The modeling methodology established in this work can provide a powerful tool for the modeling-driven design of next-generation carbon−carbon composite precursor chemistries for thermal protection systems and other high-temperature applications.

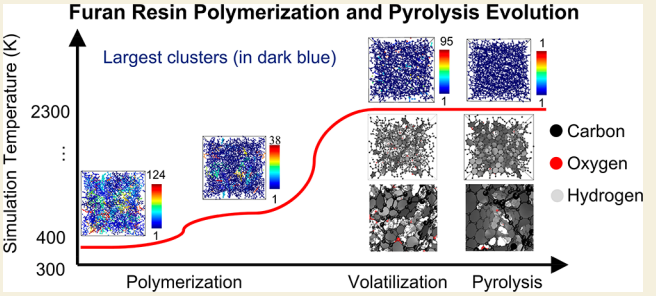

KEYWORDS: *furan resin, glassy carbon, pyrolysis, carbonization, carbon−carbon composites, thermal protective system*

1. INTRODUCTION

Glassy carbon (GC), also known as vitreous carbon, was originally synthesized in the 1930s.[1] GC differs from amorphous carbon or graphite due to its semicrystalline atomic structure. The atomic structure gives this material unique properties such as excellent electrical conductivity, biocompatibility, chemical inertness, thermal stability, low mass density, and relatively high Young's modulus.[1,2] Because of these properties, GC is extensively used in ablatives, carbon−carbon composites (C/C composites), electrodes, bone implants, and synthetic zeolites, to name a few applications.[1,3−7] C/C composites are particularly relevant to the development of the next generation of hypersonic vehicles that require lightweight and thermally resistant structural components. However, the process parameters used to manufacture this material, which play a critical role in the resulting morphology and the final properties of the material, have proven difficult to optimize systematically.

GC properties are heavily influenced by the chemistry of the precursor polymer.[6] During the pyrolysis process, at elevated temperatures and in an inert atmosphere, most of the heteroatoms are removed in the form of volatiles. The characteristics of this evolving structure are highly dependent on the processing conditions and precursor chemistry.[2] The development of next-generation GC-based materials, such as C/C composites, is complicated by several factors. The many possible combinations of processing conditions and precursor chemistries mean GC materials have a large design space, which is difficult to fully explore experimentally due to cost and time constraints. Additionally, GCs exhibit length-scale-dependent elastic properties, and their final microstructure is an ongoing topic of discussion with no consensus in the literature.[1,5] Furthermore, the nanostructure of GC is not fully understood or characterized.[8] To fully optimize the properties of GC in high-performance structural materials such as C/C composites, a high-throughput method is needed to discover effective precursor chemistries and processing conditions that lead to optimal pyrolysis.

There have been a variety of models proposed for GC's atomic structure starting with the graphitizing and non-graphitizing models suggested by Franklin et al.[4,9] in 1951 which view GC atomic arrangement as basic structural units that reassemble small units of graphite. Then in 1971 Jenkin et al.[1,4,10] correlated the nongraphitizing model of GC with the crystalline nature of graphite, specifically the stacking height (L_c), and the in-plane crystallite size (L_a) associated with graphitic planes. The most recent model proposed by Jurkiewicz et al.,[3] views GC atomic arrangement as curved carbon layers that resemble imperfect fullerenes.[1,4] There have been various attempts in the past to characterize GC as well as to understand the effect of processing parameters on the resulting structure and properties. There is experimental

Received: June 29, 2023
Revised: August 17, 2023
Accepted: September 18, 2023
Published: October 2, 2023

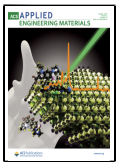

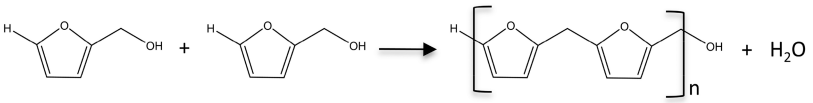

Figure 1. Most common reaction mechanism and corresponding product for PFA polymerization.

Table 1. Commonly Reported PFA Reaction Products and Corresponding Percent Moieties for Each Product Used for MD Polymerization of PFA

Arrangement	Chemical Structure	Approximate % moieties
Linear	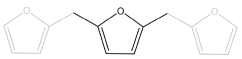	60% [29]
Ring opening		10% [29] 5% [33]
α,β-unsaturated γ-lactons	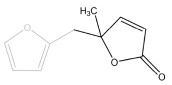	10% [29]
Conjugated	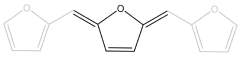	17% [33]
Diels-Alder	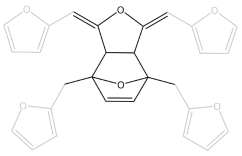	
Diels-Alder + Ring opening	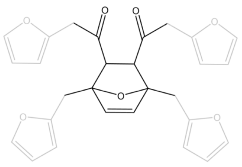	20% [29]

evidence that higher processing temperatures during pyrolysis lead to higher carbon content, higher sp^2 carbon content, and more crystalline morphologies. However, this increase does not always correspond to higher Young's modulus of the mesoscale material.[1,2,11,12] Both the experimental characterization and proposed models have yet to provide a comprehensive understanding of GC and how to tailor GC properties for specific uses. Moreover, there is a lack of understanding of how different processing conditions of GC and the resulting properties can affect the mesoscale C/C composite properties.

Integrated computational materials engineering (ICME) has recently been applied to polymer matrix composites (PMCs) to tailor the cure cycles of the composite for different applications.[13−21] The ICME approach uses properties computed from nanoscale molecular dynamics (MD) simulations in which properties are determined as a function of cure. The nanoscale properties, provided by MD for ICME and PMC optimization are the degree of cure, density, shrinkage, elastic properties, and thermal properties. It is of interest to extend the ICME approach to C/C composite manufacturing to tune the processing conditions that affect the final C/C composite performance. The first step toward extending the ICME approach to C/C composites is the development of experimentally validated MD models of GC.

There have been a variety of attempts to use MD to model carbonization and graphitization processes such as Jian et al.[22] who used a representative proxy precursor method to understand what reaction mechanisms may occur for carbon fiber synthesis. Zhang et al.[23] also used a representative proxy precursor to understand the thermal conductivity changes during different pyrolysis states. However, the proxy precursor method does not allow for a complete understanding of shrinkage that occurs as the polymer evolves into a GC structure due to the oversimplification of the proxy precursor chemistry. Nor can the proxy precursor method cannot quantify the elastic properties before pyrolysis and the initial stages of pyrolysis. Purse et al.[24] modeled phenolic resin polymerization and pyrolysis with gas removal to find char yield, Young's modulus, reaction mechanics, and thermal conductivity for different pyrolysis temperatures, but the mass densities of the model lack experimental validation. Gissinger et al.[25] recently found that MD simulations could be used to predict the char yield of a variety of different precursors via an implementation of a novel MD in silico volatile removal algorithm.

To the authors' knowledge, there has been no MD study of GC pyrolysis that generates an experimentally validated structure that can be subsequently used in an ICME process

https://doi.org/10.1021/acsaenm.3c00360
ACS Appl. Eng. Mater. 2023, 1, 2555−2566

modeling approach for C/C composites. Furthermore, the difficulty of experimentally characterizing GC presents a unique challenge of bridging the MD model to a physical sample for use in an ICME process modeling approach. ICME process modeling for PMCs has used the degree of cure (experimental) and cross-link density (MD) to link the MD models to the experiment. A linking metric that can relate a physical sample and the MD model still needs to be discovered for GC modeling integration into an ICME approach for C/C composites. The objective of this research is to establish experimentally validated reactive MD simulation protocols for the efficient and accurate prediction of the evolving physical and mechanical properties of the GC materials. The simulation protocols can be used to facilitate model-driven development of the future generation of C/C composites for hypersonic structural applications once integrated into an ICME process modeling approach. The developed MD protocols are applied to model the structural evolution of furan resin during the polymerization and pyrolysis processes. The experimental component of this work was undertaken to provide mass density and Young's modulus data to validate the MD polymerization models.

Furan resin is a thermoset polymer produced from the polymerization of furfuryl alcohol (FA) in the presence of heat and a catalyst. FA is derived from waste vegetable biomass, making FA, and consequently furan resin, or poly furfuryl alcohol (PFA), a renewable and environmentally friendly material.[6,26] PFA has found uses in the production of GC, adhesives, binders for foundry molds, corrosion protection, C/C composites, and fully biobased composites.[26−28] Despite the wide range of applications of PFA, its fundamental polymerization chemistry is complex and is not fully understood by the scientific community. Processing conditions, such as the heat and catalysts used, as well as processing times and storage methods of the FA monomer, all effect the final polymerized structure.[26,29−31] Due to the sensitivity of PFA polymerization to processing conditions, there are many reaction mechanisms and corresponding products that may or may not contribute to the production of a particular cured sample. FA polymerization is dominated by the polycondensation reaction shown in Figure 1.

Several other products are thought to contribute to the fully polymerized structure and are shown in Table 1.[6,30,32,33] The prevalence of each reaction product is reported in the last column. Other potential mechanisms and products have been postulated in the literature but are not incorporated in the current MD simulations.[28,34,35]

During experimental pyrolysis, volatiles are released and pores form in the GC material, reducing the mass density of the product. Polymer-infiltration-pyrolysis (PIP) cycles can be used to densify the GC material and reduce open porosity. PIP cycles can be repeated any number of times until the desired mass density is achieved. Bulk mass densities of GC range between 1.5 and 1.9 g/cm^3.[2] Typical pyrolysis temperatures range between 1000 and 1500 K, which produces GC-material consisting mainly of carbonaceous material with a crystalline nature dependent on the precursor chemistry.[6,36] Various metrics have been used to characterize GC, which are summarized in Table 2 and will be referred to as GC characteristics throughout the rest of the discussions.

Char Yield (C_y) is the measure of mass retention during pyrolysis and can be calculated as a ratio of the mass of the evolved char to the mass of the initial polymer system:

Table 2. PFA-Derived GC Characteristics of Interest with Corresponding Temperature Range

Metric	T (K)	Experimental value
Char yield (%)	1000	50−60[6]
Interplanar crystallite spacing d_{002} (Å)	1100−1500	3.7−3.8[11,12]
In-plane crystallite size L_a (Å)	1100−1500	15−18[12]
Out-of-plane crystallite stacking height L_c (Å)	1100−1500	10[12]
Carbon content (%)	1000−1700	94−98[2]
sp^2 carbon content (%)	1000−1700	95−98[2]

$$C_y = \frac{\text{mass}_{\text{char}}}{\text{mass}_{\text{polymer}}} \quad (1)$$

The interplanar spacing (d_{002}), the stacking height (L_c), and the crystallite width (L_a) of graphitic planes can be experimentally determined by X-ray diffraction (XRD) and give insight into the morphology and crystallinity of the GC material. d_{002} is computed using Bragg's law and the associated (002) reflection angle

$$D = \frac{\lambda}{2\sin(\theta)} \quad (2)$$

where λ is the characteristic Cu−Kα radiation wavelength of 1.54 Å.[12,37] L_a and L_c are computed by using the Scherrer equation:

$$L = \frac{K\lambda}{\beta\cos(\theta)} \quad (3)$$

L_a is computed from the diffraction peaks associated with the (100) planes and L_c is computed from the diffraction peaks associated with the (002) planes. β is the full width at half-maximum of the peak used to compute L_a and L_c.[12,37]

2. METHODS

All MD results presented here were obtained with the LAMMPS (Large-Scale Atomic/Molecular Massively Parallel Simulator) 2020 software package[38] and used the ReaxFF force field to model interatomic interactions as implemented in LAMMPS via the "*pair reaxff*" command. The "*fix qeq/reax*" command was used to enable atomic charges to vary during the simulation in response to bonding changes using a charge equilibration algorithm.[39,40] All MD simulations were performed with a 0.1 fs time step, and charges were equilibrated every time step using a low taper radius cutoff of 0 Å, a high taper radius cutoff of 10 Å, and a charge tolerance of 1.0e^{-6}. The entire MD study was performed in two main stages: polymerization and pyrolysis, which are detailed in sections 2.2 and 2.3, respectively.

The bonding evolution of all MD models was tracked via the bond order output provided by the "*fix reaxff/bonds*" command in LAMMPS. All bonding analyses performed used this bond order information in combination with the standard LAMMPS datafile to interpret bonding. All bonding analyses had bond orders sampled for 0.1 ps in 0.01 ps intervals in the corresponding ensembles, temperatures, and pressures at various stages of modeling. The bond orders were averaged together and a minimum bond order cutoff of 0.3 was used to decide if the bond is strong enough to be considered as a bond. A secondary criterion was also enforced that the number of bonded neighbors per element could not exceed the valence number of the element (for example the valence number of carbon is 4, so a maximum number of bonded neighbors for all carbon atoms of 4 was enforced). If an atom of a specific element had more bonded neighbors than the valence number, the weakest bonds were rejected.

https://doi.org/10.1021/acsaenm.3c00360
ACS Appl. Eng. Mater. 2023, 1, 2555−2566

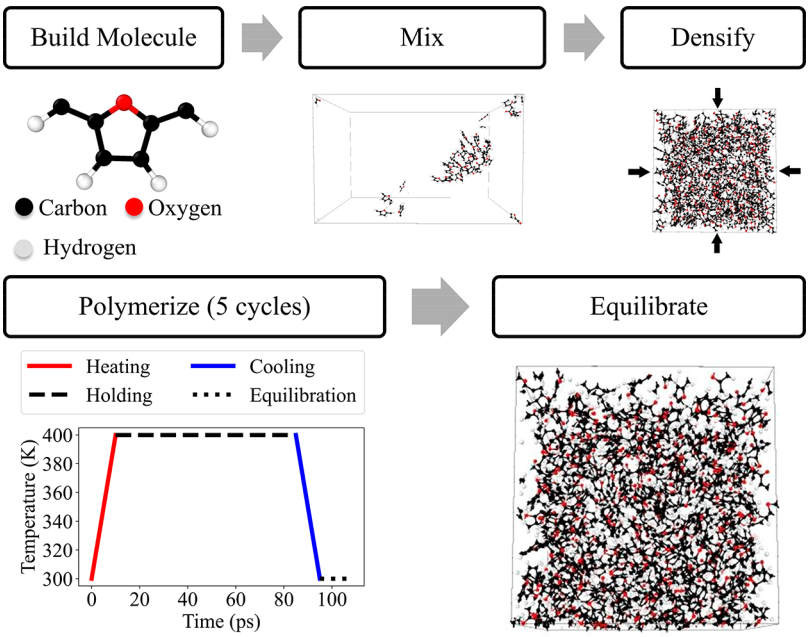

Figure 2. MD model building workflow used to polymerize PFA in ReaxFF.

Table 3. PFA starting Molecules with Open Valence Atoms Are Colored Red and the Mix Counts for Each Molecule

Arrangement	Chemical Structure	Mix count
Conjugated + Linear	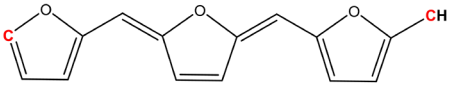	2
Ring opening + Linear	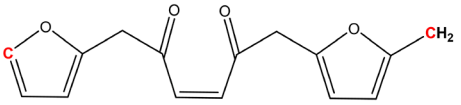	2
Conjugated	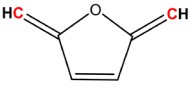	5
Diels-Alder + Linear	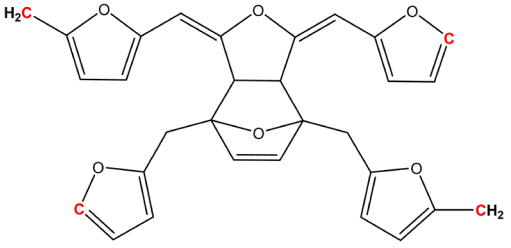	4

2.1. Experimental Polymerization

PFA was synthesized by polymerization of FA. An aqueous *p*-toluenesulfonic acid catalyst solution was obtained by adding 1.0 g of *p*-toluenesulfonic acid to 14.5 mL of water at 298 K. The acid catalyst solution was mixed gently with a glass stir rod for 1 min. The acid catalyst solution was added dropwise to 300 mL of FA monomer with constant gentle manual stirring using a glass rod at 298 K. The mixture was poured into a silicone mold to produce specimens with dimensions of 3 mm thickness, 25 mm width, and 178 mm length. The mold was placed into an oven, and the mixture was cured at 313 K under atmospheric pressure for 96 h. The oven temperature was then raised to 373 K and held for 1 h and then raised again to 443 K and held for 1 h. Afterward, the oven was turned off and the mixture was allowed to cool to 298 K overnight.

2.2. Simulated Polymerization

The polymerization of PFA was performed using the CHON-17_Weak parameter set due to its demonstrated ability to accurately predict mass density and elastic properties.[41,42] Five statistically different, relatively small models (referred to as "replicates" hereafter) of 4860 atoms were built, as well as a single larger system of 32,400 atoms. An open valence approach was used to enhance the reactivity and accelerate the polymerization process by placing undercoordinated atoms at certain locations in the reactant molecules. The relative amount of each precursor molecule was chosen to match the percentages found in experimental work by Tondi et al.[29] and

https://doi.org/10.1021/acsaenm.3c00360
ACS Appl. Eng. Mater. 2023, 1, 2555−2566

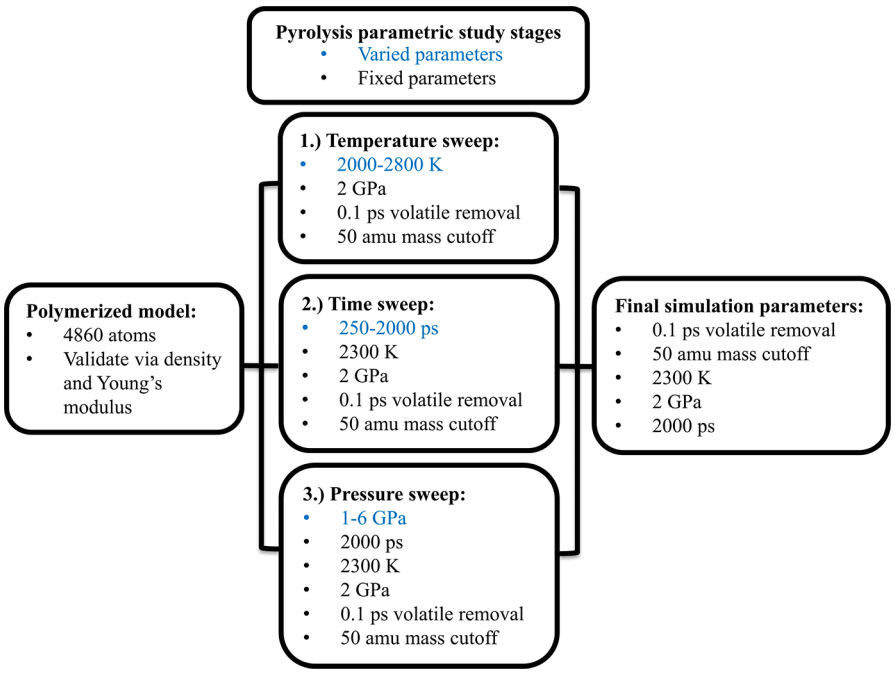

Figure 3. MD model pyrolysis parametric study used to find the MD simulation settings that could best predict the experimental GC characteristics. The parameters labeled in blue vary at each step of the parameter optimization, while the parameters labeled in black are fixed.

Shibutani et al.,[33] summarized in Table 1. The polymerization workflow is shown in Figure 2 (molecules visualized in OVTIO[43]).

The initial molecules were built and minimized in ChemDraw 3D and then converted to a LAMMPS datafile with the atomic partial charges set to zero. The starting molecules were mixed in specific molar ratios (Figure 2) at a low density of 0.35 g/cm^3 and heated from 1 to 300 at 10 K/ps to allow the molecules to adjust to the ReaxFF potential and to allow the charges to be equilibrated in the canonical ensemble (NVT). Subsequent 300 K NVT simulations were initialized with random velocity seeds for each of the five replicates and the large system to produce statistically independent models. The mixed molecules were then replicated, and the simulation cell dimensions were uniformly reduced at 300 K in the NVT ensemble until the mass density reached 1.13 g/cm^3, the experimental density of uncured FA.[44] The densified system was subjected to five sequential heating-holding-cooling-equilibration cycles to polymerize the system. The heating and cooling stage temperatures were ramped at 10 K/ps, and the equilibration stage was performed at 300 K and 1 atm in the constant pressure, constant temperate ensemble (NPT) for 10 ps. The holding stage was performed for 75 ps at 400 K in NVT, which is the reported processing temperature for PFA.[45] Finally, the polymerized models were simulated at 300 K and 1 atm for 500 ps in the NPT ensemble to allow the final polymerized structure to fully equilibrate. The starting furan molecules, mixing count, and associated open valence locations are listed in Table 3.

The starting molecules were carefully constructed to help incorporate the features observed by Tondi et al.[29] and Shibutani et al.[33] Tondi et al. determined that 20% of their cured samples were formed via a Diels–Alder ring-opening reaction, while Shibutani et al. found that approximately 17% of their cured samples had conjugated furan rings. To incorporate the observations of Shibutani et al. into the current work, the Diels–Alder bonding configuration with a closed ring (Table 1) was used, since this Diels–Alder reaction involves a conjugated furan ring. The mixing ratio of each molecule was established by attempting to match the moiety percent of the starting molecules to those shown in Table 1. The resulting percent moiety breakdown of the starting molecules used in the simulations is 58.54% linear, 19.51% Diels–Alder, 4.89% ring-opening, and 17.06% conjugated. Two metrics were used to track and quantify the cure evolution of the system. The first metric was the largest cluster mass ratio, which is the mass of the largest cluster of bonded atoms divided by the entire system mass. The second metric was the extent of the reaction for polycondensation reactions:[46]

$$p = \frac{N_0 - N}{N_0} \tag{4}$$

where p is the extent of reaction (conversion), N_0 is the initial number of molecules before polymerization, and N is the number of reacted molecules at any point throughout the polymerization process. For this study, the largest cluster percent mass and extent of reaction data were computed at the end of each equilibration stage in the polymerization cycle of Figure 2 (every 105 ps due to the heating-holding-cooling-equilibration simulation time of each cycle).

Once the largest cluster mass ratio and extent of reaction converged with respect to the simulation run time, the mass density and Young's modulus for each replicate were computed for model validation. The mass density was computed by averaging the last 250 ps of LAMMPS density data from the equilibration stage (Figure S1). The Young's modulus was determined by applying uniaxial strain to each equilibrated model in the 3 principal directions at a strain rate of 10 ns^{-1}. The uniaxial strain simulation occurred at 300 K and 1 atm using the NPT ensemble, which employed both the Nosé–Hoover barostat and thermostat and allowed Poisson's contraction to occur in the transverse directions. The normal stress in the simulation was computed using the LAMMPS "*compute pressure*" command, which provides a symmetric pressure tensor. The Young's modulus was computed by fitting linear regression lines to the initial linear region of the stress–strain response and is shown in Figure S1.[47]

2.3. Simulate Pyrolysis

The simulated pyrolysis of the polymerized and equilibrated PFA models was performed using the CHON19 parameter set due to its demonstrated ability to accurately model char formation in hydrocarbon materials.[48] The CHON19 carbon parametrization used existing carbon parameters from the Srinivasan parameter set[49] developed for graphene/fullerene materials, which should allow it to work well for predicting the mechanical properties of partially graphitic materials.[48] To simulate the off-gassing of volatile species during the pyrolysis process, the "*fix reaxff/species delete*" command in LAMMPS, developed by Gissinger et al.,[25] was used to identify (based on bond-order averaging) and remove the small molecules in the system. The bond orders in the system were sampled every time step

https://doi.org/10.1021/acsaenm.3c00360
ACS Appl. Eng. Mater. 2023, 1, 2555–2566

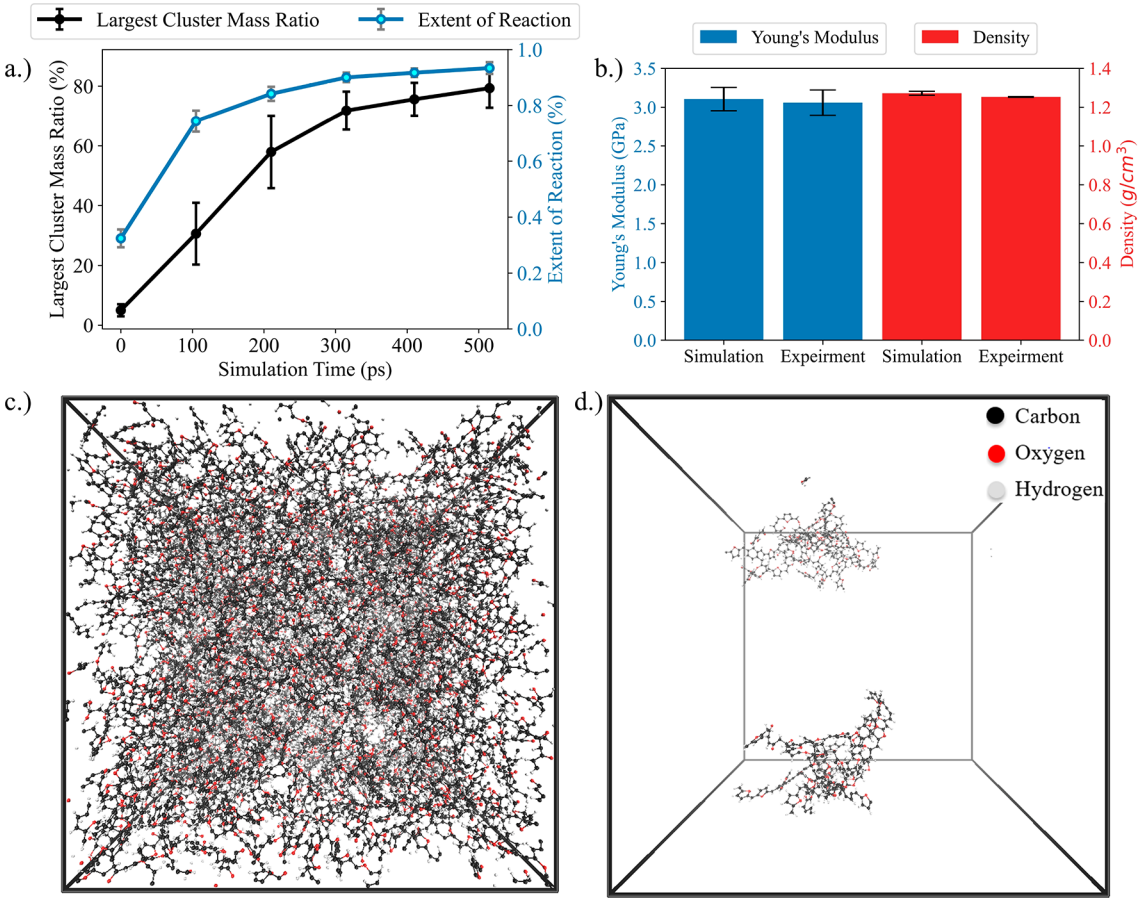

Figure 4. Polymerization metrics determined using the modeling procedure from section 2.2 Simulated polymerization: (a) Largest cluster mass ratio and Extent of reaction evolution average for all simulated models. Convergence indicates that most chemical reactions have occurred. (b) Simulated and experimental density and Young's modulus results for polymerized PFA. (c) First largest cluster. (d) Second largest cluster.

and averaged over 0.01 ps to find the mass of volatile molecules, and a mass limit of 50 amu was used remove common furan pyrolysis volatiles such as H_2O, CH_4, CO, CO_2, and H_2.[6] For each time step in which volatiles were removed from the system, all molecules under 50 amu were removed with no rate of removal defined.

To accurately develop MD models of GC to be used in an ICME process modeling approach, the MD-predicted properties must match experimental properties. In this work, the MD predicted Young's modulus of the GC material have been compared to that of ultrathin carbon materials because sample size and Young's modulus are known to be inversely correlated in GC,[2,5,50] likely due to the presence of larger pores or defects in larger samples. The MD-predicted density is compared to the experimental skeletal density of pyrolyzed PFA. Experimental skeletal density removes the contribution of open pore volume, as determined by standard helium pycnometer methods, from the calculation. The skeletal density yields a density value more reflective of the nanoscale structure of the MD GC material.[12] Therefore, both the MD-predicted density and Young's modulus are compared to the experimental values taken from the literature at the nanometer length scales.[12,50] The linear shrinkage at the nanometer length scale is also computed to compare to the approximate mesoscale shrinkage that GC-derived PFA undergoes.

The optimal MD pyrolysis settings will be determined by comparing the models to the experimental GC characteristics listed in Table 2. Once the optimal MD simulation settings are found via a parametric study, they will be used to pyrolyze all models. To reduce the computational cost, the parametric study was performed on a smaller polymer model (4860 atoms). The pyrolysis of a large system and its comparison to a smaller system are of interest because, if there is minor difference in the results, then it would be more economical to use smaller systems for future studies (a detailed discussion of the MD simulation size can be found in the Supporting Information). The MD pyrolysis parametric study is summarized in Figure 3. Typical experimental pyrolysis temperatures range between 1000 and 1500 K.[6,36] Experimental pyrolysis also occurs within hours to days of processing, whereas MD is limited to nanoseconds. To allow the evolution of the structure to change from polymer to GC within the nanosecond time scale accessible in MD, higher temperatures and pressures are required. The higher temperatures in MD accelerate the chemical reactions, whereas the higher pressures allow the simulation density to more quickly converge to a final value.

The sp^1, sp^2, and sp^3 carbon content, the 5-membered, 6-membered, and 7-membered all-carbon rings, and the hydrogen and oxygen content (referred to as "chemical characteristics" from here and onward) were tracked during pyrolysis simulations. The chemical characteristics were analyzed every 10 ps and were expected to converge with respect to the simulation time to demonstrate that most of the reactions have occurred. The fully polymerized systems were heated at 10 K/ps in the NVT ensemble up to the pyrolysis temperature. Once at the pyrolysis temperature, the temperature and pressure were held constant using the Nosé−Hoover thermostat and barostat for 2000 ps before cooling to 300 K in NVT at a cooling rate of 10 K/ps. This was followed by a 300 K, 1 atm NPT simulation for 500 ps to equilibrate the models. Before equilibration of the models, each model was checked for any small volatiles that may have formed and were removed if present. No volatiles were observed to form after equilibration. The MD-predicted GC-material density and Young's modulus were computed in the same manner that the MD polymerized properties were computed (visualized in Figure S1). The crystallite dimensions and sizes were computed using XRD spectra provided by the LAMMPS "*compute xrd*" command.[51] The Scherrer constant K value of 0.9 adopted by Burket et al.[12] for

https://doi.org/10.1021/acsaenm.3c00360
ACS Appl. Eng. Mater. 2023, 1, 2555−2566

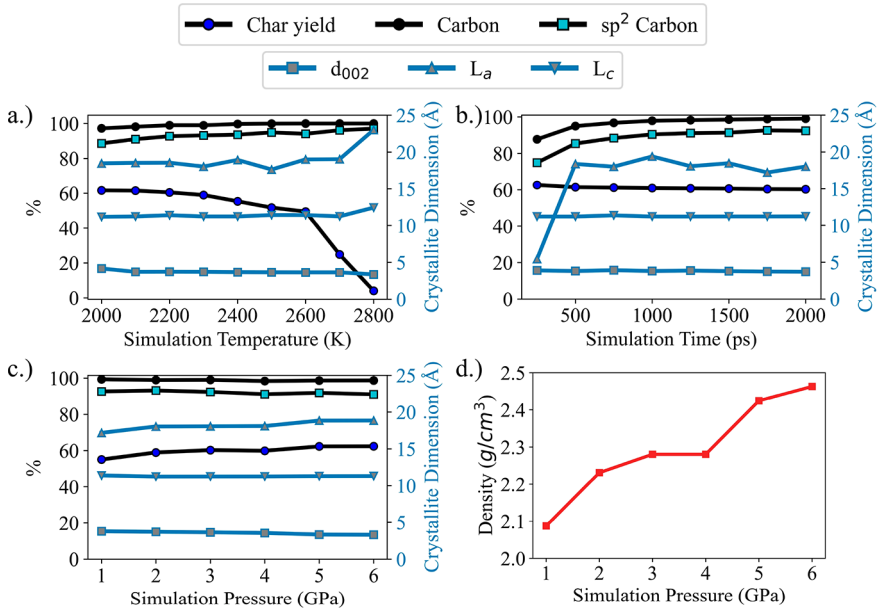

Figure 5. Parametric study of the simulation parameters. Effect of simulation (a) temperature, (b) time, and (c) pressure on predicted GC characteristics (d) pressure effect on density for the pyrolyzed MD model at 2300 K and 2000 ps.

calculating both L_a and L_c for PFA derived GC was used to compute the values for the MD models. The background was removed from the LAMMPS computed XRD spectra, and Gaussian curves were fit to the 002, 100, and 112 peaks. The max θ and β were computed from the 002 and 100 peaks to determine d_{002}, L_a, and L_c for the pyrolyzed MD models (Figure S8).

3. RESULTS AND DISCUSSION

3.1. Experimental Polymerization

The specimen densities were measured using the water buoyancy method according to the ASTM D792 density standard. The density was calculated to be 1.253 ± 0.002 g/cm^3. Specimens were then evaluated for elastic properties at 296 K according to ASTM D638 tensile standard using the ASTM Type I sample geometry: 65 mm long × 3.2 mm thick. The cured specimens were machined into dog-bone-shaped samples with a width of 12.6 mm by using a Ceast table router. Samples were tested at a crosshead rate of 1 mm/min using an Instron 4206 screw-driven mechanical testing machine. Strain values were measured with a 50.8 mm Epsilon axial extensometer. Young's modulus was determined from the initial slope of the stress−strain curve. Six tensile tests were performed, and the Young's modulus was found to be 3.059 ± 0.163 GPa.

3.2. Simulated Polymerization

The largest cluster mass ratio and the extent of reaction for all models converged after 5 polymerization cycles (515 ps) and are shown in Figure 4a. The data indicate that further simulation time would not lead to any further reactions, thus marking the end point for the polymerization stage. The average largest cluster mass ratio percent reached 79.3%, and the average extent of reaction reached 86.0%. The largest cluster contains most of the atoms and fills most of the simulation cell as shown in Figure 4c. The second largest cluster shown in Figure 4d is much smaller than the first largest cluster. After the polymerization was complete, the average equilibrated mass density was found to be 1.272 ± 0.010 g/cm^3, which agrees well with the experimentally determined value (Figure 4b) and the literature value of 1.27 g/cm^3.[11] The average MD Young's modulus was 3.1 ± 0.2 GPa, which also agrees well with the experimentally determined Young's modulus (Figure 4b) despite the different strain rates used in the experiment and MD simulation. The larger strain rates used in MD means that it is possible that the MD predicted mechanical properties are higher due to the inability of the molecular chains to relax during the strain simulations. Li et al.[52] observed that Young's modulus computed by MD for amorphous polymers is insensitive to the applied strain rate, whereas the MD computed yield strength has a larger dependence on the applied strain rate. The MD data of Patil et al.[14] show the same findings for amorphous polymers and the strain rate sensitivity of predicted mechanical properties. As the polymer evolved from a liquid to the final polymerized state the average nanometer length scale linear shrinkage was found to be 3.72 ± 0.25%.

3.3. Simulate Pyrolysis

The initial combination of pyrolysis settings in the parametric study consisted of a volatile deletion interval of 0.1 ps, 50 amu mass cutoff for volatile removal, 2000 K processing temperature, and a processing pressure of 2 GPa. After 2000 ps of simulation time, the convergence of the chemical characteristics indicated that the chemical conversion process was essentially complete. The convergence of all tracked chemical characteristics indicated that a simulation time of 2000 ps was sufficient. An example convergence graph for a smaller model can be seen in Figure S2a, where all chemical characteristics converged after 2000 ps of simulation time.

The GC characteristics as a function of temperature were computed after 2000 ps of simulation time and are seen in Figure 5a. The simulation temperature of 2300 K best matches these GC characteristics, whereas lower temperatures result in lower than desired sp^2 carbon content and higher temperatures create lower than desired char yield and higher than desired L_a size. Thus, 2300 K will be used for the remainder of the simulations. The temperature effects on the crystallite size found experimentally by Burket et al.[12] indicate that higher

https://doi.org/10.1021/acsaenm.3c00360
ACS Appl. Eng. Mater. 2023, 1, 2555−2566

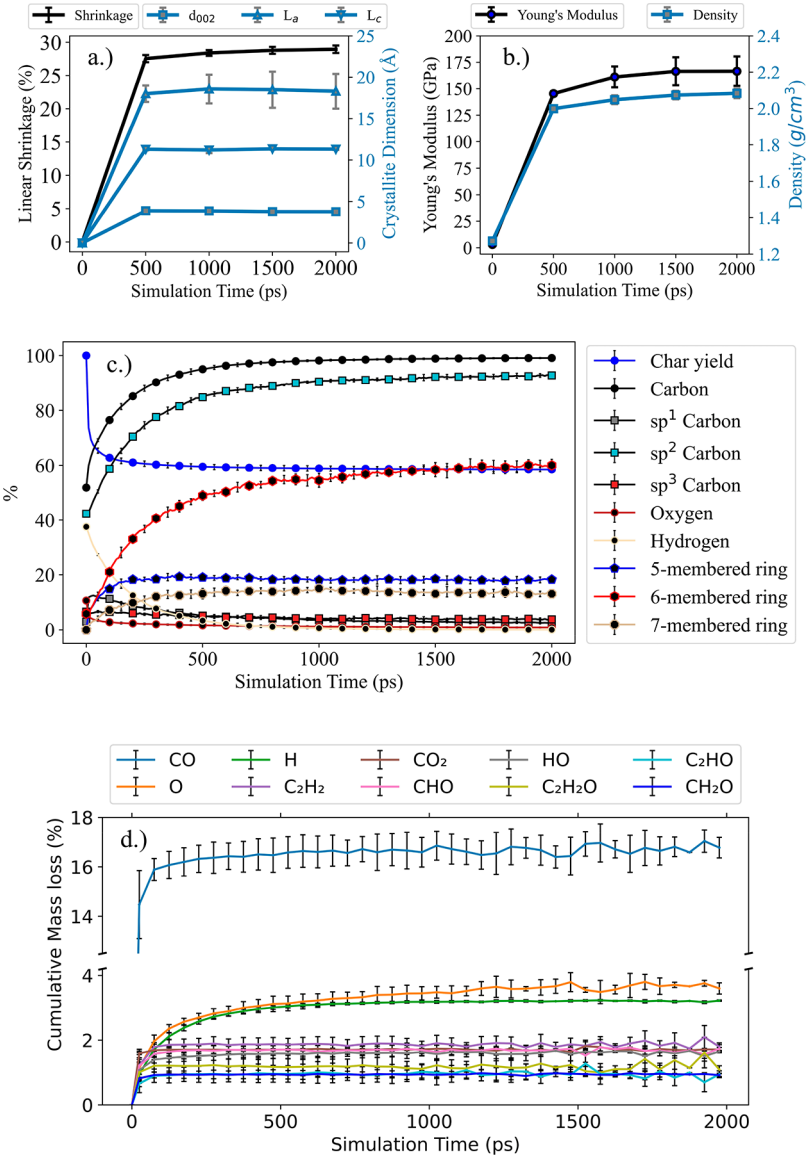

Figure 6. Evolution during pyrolysis. (a) Shrinkage and crystallite dimensions of all MD models. (b) Physical property evolution of all MD models. (c) Chemical characteristics evolution of all MD models. The lines have data points every 10 ps, and markers/error bars are plotted every 120 ps. (d) Cumulative volatile mass loss evolution between all models. (Legend is ordered highest mass loss ratio to smallest mass loss, showing the 10 most frequently removed volatiles.)

temperatures decrease the d_{002} spacing, increase the L_a in-plane dimensions, and increase the L_c out-of-plane stacking height. The temperature-crystallite size effect is reflected in the data presented in Figure 5a, where the increase in the temperature resulted in smaller d_{002} values and increased L_a and L_c values. Next, a study of simulation time was performed at 2300 K, 2 GPa, and a volatile removal interval of 0.1 ps to confirm the GC characteristics have enough time to converge at the new processing temperature. The evolution of the GC characteristics during the simulation is shown in Figure 5b. After 1750 ps, there was negligible change in GC characteristics, concluding that 2000 ps of simulation time is sufficient.

Finally, the effect of simulation pressure was studied after 2000 ps of simulation time, a temperature of 2300 K, and a volatile removal interval of 0.1 ps. Six pressures ranging from 1 to 6 GPa were simulated, and the resulting predicted GC characteristics are shown in Figure 5c. The data in the figure demonstrate that the simulation pressure had a negligible effect on the resulting GC characteristics. The simulation pressure of 2, 3, and 4 GPa all have the same char yield value and L_a size, whereas higher pressures like 5 and 6 GPa slightly increase char yield and increase the L_a size. The simulation pressure of 1 GPa slightly decreases the char yield and L_a size. To help decide which pressure should be used, the MD model density during pyrolysis was computed at 2300 K at the different pressures by averaging the last 50 ps of density data during the 2000 ps pyrolysis and volatile removal simulation (shown in Figure 5d). The pyrolysis pressure influences the pyrolyzed system density, where an increase in the pyrolysis pressure increases the system density. Once the pyrolyzed models were cooled and equilibrated at 300 K and 1 atm, the final equilibrated density was lower than the density at the elevated pyrolysis temperature and pressure because of the temperature and pressure differences at each stage. The pyrolysis pressure of 2 GPa provided a final room temperature and pressure–density that matches the experimental skeletal density found by

https://doi.org/10.1021/acsaenm.3c00360
ACS Appl. Eng. Mater. 2023, 1, 2555−2566

Burket et al.,[12] and thus 2 GPa is the decided pyrolysis pressure.

The effect of volatile deletion intervals could not be studied because longer deletion intervals required significantly longer simulation times to reach converged chemical characteristics (Figure S2). The value of 0.1 ps was accepted as a reasonable value that permitted converged results in useful simulation run times. The parametric study concluded that the optimal simulation parameters that can predict experimental validated GC characteristics are 2300 K, 2 GPa, a volatile removal interval of 0.1 ps, a volatile mass cutoff of 50 amu, and a maximum simulation time of 2000 ps. These settings subsequently were used to pyrolyze all other models, the results of which are described below.

As observed in Figure 6a and c, there were no significant differences in the computed chemical and GC characteristics between the five smaller replicates and the large system, as indicated by the standard deviation of the average of the 6 samples. Individual convergence plots for each smaller model and the large system can be found in Figure S3. As the polymerized structure evolved into the pyrolyzed structure, the system changed significantly in terms of GC characteristics, especially with an increase in the sp^2 carbon content and the production of 5/6/7-membered all-carbon rings. The average d_{002}, L_a, and L_c values at 2000 ps of simulation time of 3.77 ± 0.07 Å, 18.00 ± 2.00 Å, and 11.30 ± 0.09 Å respectively are in reasonable agreement with experiments.[12] The average carbon content of 99.20 ± 0.20% was overpredicted,[2] while the average sp^2 carbon content of 92.80 ± 0.90% was underpredicted.[2] As the polymerized structure evolves into the pyrolyzed structure, the atomic structural rearrangements start to affect the mass density and Young's modulus (Figure 6b). The average final mass density after 2000 ps of pyrolysis of 2.08 ± 0.03 g/cm^3 agrees well with the reported skeletal density range of pyrolyzed PFA of 1.9−2.1 g/cm^3 reported by Burket et al.[12] The average final Young's modulus of 167 ± 14 GPa agrees well with the measured modulus of ultrathin carbon materials of 185 GPa.[50] The strain rate effect on the pyrolyzed structure is less of a concern as compared to the polymerized structure since there are no molecular chains but rather a completely connected fused ring sp^2 carbon structure. Such a structure will show less viscoelastic tendencies due to the stiffer arrangement of atoms. A discussion of the MD system size (number of atoms) can be found in the Supporting Information.

The cumulative volatile mass loss ratio produced by volatile removal was analyzed for each system and averaged together across all systems (Figure 6d). The cumulative volatile evolution for each model can be found in Figure S4. The results of these analyses indicate that the main volatiles removed in the simulations were CO, O, H, C_2H_2, and CO_2. Oxygen and hydrogen atoms are not expected volatiles in the experiment, which implies that longer removal intervals might be needed to allow time for secondary reactions to produce O_2, H_2, or other molecular volatiles.

Considering that the polymerized and final pyrolyzed models have been validated with experimental literature, it can be assumed that the evolution of chemical and GC characteristics as well as mechanical properties between the polymerized and final pyrolyzed states are valid as well. Most of the changes in chemical characteristics, GC characteristics, and physical properties occur within the first 500 ps (or one-quarter) of the pyrolysis process. The crystalline nature of the material is already established within the first 500 ps, whereas the sp^2 carbon content and 6-membered all-carbon rings require longer times to finish evolving. The atomic evolution of the structure is visualized in Figure 7 at different stages of pyrolysis.[53] From Figure 7 it is qualitatively observable that as the GC structure gets pyrolyzed, there is an increase in imperfect fullerene ribbons that start to template with one another creating complex interconnected free-volume pockets. The emergence of such interconnected pockets is likely due to a higher degree of sp^2 carbon and 6-membered all-carbon rings appearing in the later stages of pyrolysis.

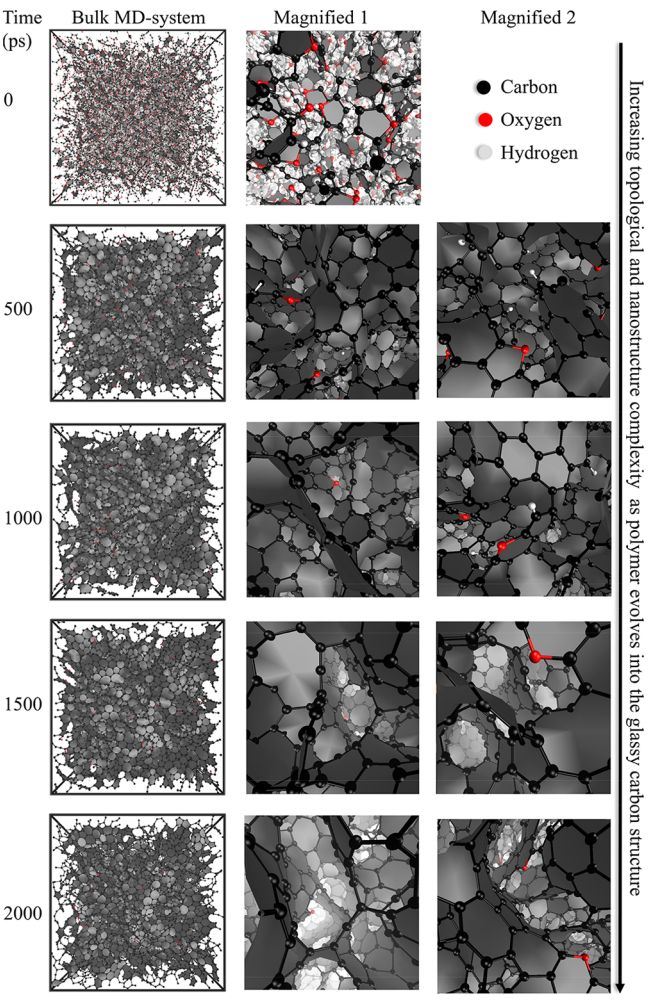

Figure 7. Structural evolution of the large system is visualized throughout the pyrolysis process.

The linear shrinkage experienced during pyrolysis is shown in Figure 6a. After 2000 ps, the linear shrinkage was found to be 28.95 ± 0.56%, which is overpredicted relative to the experimentally known value of about 20% linear shrinkage at the mesoscale.[6,11] The reason for this overprediction could be that the linear shrinkage computed with the MD models is at the nanometer length scale and excludes the effects of porosity. The combined nanometer length shrinkage due to covalent bond formation during polymerization and the complex chemical restructuring and crystallization due to pyrolysis is 32%. During C/C composite manufacturing, residual stress will build up due to this level of shrinkage, and ICME process modeling can be used to quantify the residual stress evolution.

https://doi.org/10.1021/acsaenm.3c00360
ACS Appl. Eng. Mater. 2023, 1, 2555−2566

Most of the nanoscale linear shrinkage occurs within the first 500 ps (or a quarter) of the pyrolysis process, with very few changes beyond the first 500 ps. The GC characteristics, physical properties, and shrinkage were computed every 500 ps or one-fourth of the pyrolysis process. The results of this study indicate that it would be better to discretize the pyrolysis stages in a logarithmic manner, where more frequent properties and characteristics are computed early in the pyrolysis process with respect to the simulation time. Having more frequent characteristics and properties computed early in the pyrolysis process would allow for an ICME process modeling approach to capture better resolutions of shrinkage and residual stress evolution inside a C/C composite.

4. CONCLUSIONS

A computational workflow to model the polymerization and pyrolysis of PFA was developed by using reactive molecular dynamics. The purpose of this effort was to elucidate the atomic-scale structural and chemical evolution that occurs throughout the entire process of glassy carbon production to develop inputs for the ICME process modeling. Experimental specimens of PFA were synthesized and characterized to validate the mass density and Young's modulus predicted by MD models. The predicted mass density and Young's modulus for the MD polymerized models of 1.272 g/cm^3 and 3.1 GPa show excellent agreement with experimentally measured values determined in this work of 1.25 g/cm^3 and 3.06 GPa. The predicted mass density and Young's modulus of the pyrolyzed models of 2.08 g/cm^3 and 167 ± 14 GPa agree well with the experimental values found in the literature of 1.9−2.1 g/cm^3 And 185 GPa.

A parametric study was conducted to determine the optimal MD parameters for simulating PFA pyrolysis that were experimentally validated. The optimal simulation parameters for PFA included volatile removal every 0.1 ps, a simulation temperature of 2300 K, a simulation pressure of 2 GPa, and a total simulation time of 2000 ps. Five MD replicates of 4860 atoms and one larger model of 32 400 atoms were built to determine the need for larger MD models of PFA. The results indicate that both the smaller and large PFA models simulated with ReaxFF are equally accurate at predicting the polymerized and pyrolyzed molecular structure and properties. However, it is important to note that pyrolyzed PFA has mesoscale and macroscale features at length scales far beyond those that can be simulated with MD. While this study has guided the MD simulation protocols necessary to accurately simulate PFA polymerization and pyrolysis at the nanometer length scale, a more complete model of the evolution of the PFA pyrolysis process would require a multiscale approach.

The MD models established in this work can be used to improve our understanding of the structure−property relationship throughout the evolution of PFA processing during polymerization and pyrolysis. Parameters such as the density and Young's modulus evolution obtained through this modeling can be used to optimize processing temperatures, hold times, and ramp rates for GC production derived from pyrolysis of PFA once applied in an ICME process modeling approach.[13−21] Furthermore, this work guides establishing MD simulation protocols for simulating next-generation C/C composite precursor chemistries.

The use of trademarks or names of manufacturers in this report is for accurate reporting and does not constitute an official endorsement, either expressed or implied, of such products or manufacturers by the National Aeronautics and Space Administration

■ ASSOCIATED CONTENT

Supporting Information

The Supporting Information is available free of charge at https://pubs.acs.org/doi/10.1021/acsaenm.3c00360.

Figure S1: Density and Young's modulus plots with a description. Figure S2: Pyrolysis chemical characteristics varying volatile removal times with a description. Figure S3: Pyrolysis chemical characteristics for all models studied with a description. Figure S4: Pyrolysis volatile evolution for all models studied with a description. Figure S5: Polymerization system size study for larger and smaller MD models with a description. Figure S6: GC system size study for larger and smaller MD models with a description. Figure S7: GC characteristics correlation to properties and structures with a description. Figure S8: Processed XRD spectra from LAMMPS for computing crystallite dimensions. Figure S9: Quenching rate considerations of the GC material with a description (PDF)

■ AUTHOR INFORMATION

Corresponding Author

Gregory M. Odegard − *Michigan Technological University, Houghton, Michigan 49931, United States;* orcid.org/0000-0001-7577-6565; Phone: (906)-487-2329; Email: gmodegar@mtu.edu

Authors

Josh Kemppainen − *Michigan Technological University, Houghton, Michigan 49931, United States*

Ivan Gallegos − *Michigan Technological University, Houghton, Michigan 49931, United States*

Aaron S. Krieg − *Michigan Technological University, Houghton, Michigan 49931, United States*

Jacob R. Gissinger − *NASA Langley Research Center, Hampton, Virginia 23666, United States*

Kristopher E. Wise − *NASA Langley Research Center, Hampton, Virginia 23666, United States*

Margaret Kowalik − *Pennsylvania State University, State College, Pennsylvania 16801, United States*

Julia A. King − *Michigan Technological University, Houghton, Michigan 49931, United States*

S. Gowtham − *Michigan Technological University, Houghton, Michigan 49931, United States*

Adri van Duin − *Pennsylvania State University, State College, Pennsylvania 16801, United States;* orcid.org/0000-0002-3478-4945

Complete contact information is available at: https://pubs.acs.org/10.1021/acsaenm.3c00360

Author Contributions

Josh Kemppainen: Conceptualization, Methodology, Software, Validation, Writing. Ivan Gallegos: Conceptualization, Methodology, Validation, Writing−review. Aaron S. Krieg: Data curation, Formal analysis. Jacob R. Gissinger: Conceptualization, Methodology, Software, Writing−review and editing. Kristopher E. Wise: Conceptualization, Methodology, Supervision, Writing−review and editing. Margaret Kowalik:

Conceptualization, Methodology, Supervision, Writing−review and editing. Julia A. King: Conceptualization, Methodology, Supervision. Gregory M. Odegard: Supervision, Funding acquisition, Writing−review and editing. Adri van Duin: Conceptualization, Writing−review and editing. S. Gowtham: Software.

Notes

The authors declare no competing financial interest.

■ ACKNOWLEDGMENTS

This research was partially supported by the NASA Space Technology Research Institute (STRI) for Ultra-Strong Composites by Computational Designs (US-COMP), grant NNX17AJ32G, as well as by the Sam M. Cohodas scholarship. SUPERIOR, a high-performance computing cluster at Michigan Technological University, was used in obtaining the MD simulation results presented in this publication.

■ ABBREVIATIONS

GC, glassy carbon; C/C composites, carbon−carbon composites; ICME, integrated computational materials engineering; PMCs, polymer matrix composites; MD, molecular dynamics; FA, furfuryl alcohol; PFA, poly furfuryl alcohol; PIP, polymer infiltration pyrolysis; XRD, X-ray diffraction

■ REFERENCES

(1) Uskoković, V. A historical review of glassy carbon: Synthesis, structure, properties and applications. *Carbon Trends* **2021**, *5* (2021), 100116.

(2) Jurkiewicz, K.; Pawlyta, M.; Zygadło, D.; Chrobak, D.; Duber, S.; Wrzalik, R.; Ratuszna, A.; Burian, A. Evolution of glassy carbon under heat treatment: correlation structure−mechanical properties. *J. Mater. Sci.* **2018**, *53* (5), 3509−3523.

(3) Jurkiewicz, K.; Duber, S.; Fischer, H. E.; Burian, A. Modelling of glass-like carbon structure and its experimental verification by neutron and X-ray diffraction. *J. Appl. Crystallogr.* **2017**, *50* (1), 36−48.

(4) Vieira, L. d. S. A review on the use of glassy carbon in advanced technological applications. *Carbon* **2022**, *186* (2022), 282−302.

(5) Manoharan, M. P.; Lee, H.; Rajagopalan, R.; Foley, H. C.; Haque, M. A. Elastic properties of 4−6 nm-thick glassy carbon thin films. *Nanoscale Res. Lett.* **2010**, *5* (1), 14−19.

(6) Savage, G. *Carbon−Carbon Composites*, 1st ed.; Chapman & Hall, 1993.

(7) Wang, H.; Yao, J. Use of poly(furfuryl alcohol) in the fabrication of nanostructured carbons and nanocomposites. *Industrial & engineering chemistry research* **2006**, *45* (19), 6393−6404.

(8) Jurkiewicz, K.; Duber, S.; Burian, A. Paracrystalline structure of glass-like carbons. *International Journal of Applied Glass Science* **2016**, *7* (3), 355−363.

(9) Franklin, R. E. Crystallite growth in graphitizing and non-graphitizing carbons. *Proc. R.Soc. London, Ser. A.* **1951**, *209*, 1097, DOI: 10.1098/rspa.1951.0197.

(10) Jenkins, G. M.; Kawamura, K. Structure of glassy carbon. *Nature* **1971**, *231* (5299), 175−176.

(11) Kim, J.; Kim, M.-S.; Hahm, H.-S.; Lim, Y.-S. Structural and property changes in glass-like carbons formed by heat treatment and addition of filler. *Macromol. Res.* **2004**, *12* (4), 399−406.

(12) Burket, C. L.; Rajagopalan, R.; Marencic, A. P.; Dronvajjala, K.; Foley, H. C. Genesis of porosity in polyfurfuryl alcohol derived nanoporous carbon. *Carbon* **2006**, *44* (14), 2957−2963.

(13) Gaikwad, P. S.; Krieg, A. S.; Deshpande, P. P.; Patil, S. U.; King, J. A.; Maiaru, M.; Odegard, G. M. Understanding the origin of the low cure shrinkage of polybenzoxazine resin by computational simulation. *ACS Appl. Polym. Mater.* **2021**, *3* (12), 6407−6415.

(14) Patil, S. U.; Shah, S. P.; Olaya, M.; Deshpande, P. P.; Maiaru, M.; Odegard, G. M. Reactive molecular dynamics simulation of epoxy for the full cross-linking process. *ACS Appl. Polym. Mater.* **2021**, *3* (11), 5788−5797.

(15) Odegard, G. M.; Patil, S. U.; Deshpande, P. P.; Kanhaiya, K.; Winetrout, J. J.; Heinz, H.; Shah, S. P.; Maiaru, M. Molecular dynamics modeling of epoxy resins using the reactive interface force field. *Macromolecules* **2021**, *54* (21), 9815−9824.

(16) Maiaru, M. Effect of uncertainty in matrix fracture properties on the transverse strength of fiber reinforced polymer matrix composites. Presented at the *2018 AIAA/ASCE/AHS/ASC Structures, Structural Dynamics, and Materials Conference*, 2018.

(17) D'Mello, R. J.; Waas, A. M.; Maiaru, M.; Koon, R.Integrated computational modeling for efficient material and process design for composite aerospace structures. Presented at *AIAA Scitech 2020 Forum*; AIAA, 2020; AIAA2020-0655.

(18) Deshpande, P. P.; Shah, S. P.; Kashmari, K.; Olaya, M.; Odegard, G. M.; Maiaru, M.. Multiscale modelling of the cure process in thermoset polymers using ICME. In *Proceedings of the American Society for Composites 35th Conference*; American Society for Composites, 2020.

(19) Shah, S.; Maiaru, M. Microscale analysis of virtually cured polymer matrix composites accounting for uncertainty in matrix properties during manufacturing. In *Proceedings of the American Society for Composites 33rd Conference*, American Society for Composites, 2018.

(20) Shah, S.; Patil, S.; Deshpande, P.; Krieg, A.; Kashmari, K.; Al Mahmud, H.; King, J.; Odegard, G. M.; Maiaru, M. Multiscale Modeling for Virtual Manufacturing of Thermoset Composites. Presented at *AIAA Scitech 2020 Forum*; AIAA, 2020.

(21) Shah, S. P.; Patil, S. U.; Hansen, C. J.; Odegard, G. M.; Maiarù, M. Process modeling and characterization of thermoset composites for residual stress prediction. *Mechanics of Advanced Materials and Structures* **2023**, *30* (3), 486−497.

(22) Jian, C.; Adams, J. J.; Grossman, J. C.; Ferralis, N. Carbon fiber synthesis from pitch: Insights from ReaxFF based molecular dynamics simulations. *Carbon* **2021**, *176* (2021), 569−579.

(23) Zang, X. Laser-engineered heavy hydrocarbons: Old materials with new opportunities. *Sci. Adv.* **2020**, *6* (17), 2020.

(24) Purse, M.; Holmes, B.; Sacchi, M.; Howlin, B. Simulating the complete pyrolysis and charring process of phenol−formaldehyde resins using reactive molecular dynamics. *J. Mater. Sci.* **2022**, *57* (15), 7600−7620.

(25) Gissinger, J. R.; Zavada, S. R.; Smith, J. G.; Kemppainen, J.; Gallegos, I.; Odegard, G. M.; Siochi, E. J.; Wise, K. E. Predicting char yield of high-temperature resins. *Carbon* **2023**, *202* (1), 336−347.

(26) Falco, G.; Guigo, N.; Vincent, L.; Sbirrazzuoli, N. Opening furan for tailoring properties of bio-based poly(furfuryl alcohol) thermoset. *ChemSusChem* **2018**, *11* (11), 1805−1812.

(27) Choura, M.; Belgacem, N. M.; Gandini, A. Acid-catalyzed polycondensation of furfuryl alcohol: mechanisms of chromophore formation and cross-linking. *Macromolecules* **1996**, *29* (11), 3839−3850.

(28) Kim, T.; Assary, R. S.; Marshall, C. L.; Gosztola, D. J.; Curtiss, L. A.; Stair, P. C. Acid-catalyzed furfuryl alcohol polymerization: characterizations of molecular structure and thermodynamic properties. *ChemCatChem.* **2011**, *3* (9), 1451−1458.

(29) Tondi, G.; Cefarin, N.; Sepperer, T.; D'Amico, F.; Berger, R. J. F.; Musso, M.; Birarda, G.; Reyer, A.; Schnabel, T.; Vaccari, L. Understanding the polymerization of polyfurfuryl alcohol: ring opening and diels-alder reactions. *Polymers* **2019**, *11* (12), 2126.

(30) Iroegbu, A. O.; Hlangothi, S. P. Effects of the type of catalyst on the polymerisation mechanism of furfuryl alcohol and its resultant properties. *Chemistry Africa* **2018**, *1* (3−4), 187−197.

(31) Principe, M.; Martínez, R.; Ortiz, P.; Rieumont, J. The polymerization of furfuryl alcohol with p-toluenesulfonic acid: photocross-linkeable feature of the polymer. *Polímeros* **2000**, *10* (1), 08−14.

(32) Shindo, A.; Izumino, K. Structural variation during pyrolysis of furfuryl alcohol and furfural-furfuryl alcohol resins. *Carbon* **1994**, *32* (7), 1233−1243.

(33) Shibutani, K.; Nakai, J.; Aphichartsuphapkhajorn, K.; Kayaki, Y.; Kuwata, S.; Arao, Y.; Kubouchi, M. The activation of furfuryl alcohol polymerization by oxygen and its enhanced mechanical properties. *J. Appl. Polym. Sci.* **2021**, *138* (17), 1−10.
(34) Kherroub, D. E.; Belbachir, M.; Lamouri, S. Synthesis of poly(furfuryl alcohol)/montmorillonite nanocomposites by direct in-situ polymerization. *Bulletin of Materials Science* **2015**, *38* (1), 57−63.
(35) González, R.; Martínez, R.; Ortiz, P. Polymerization of furfuryl alcohol with trifluoroacetic acid: the influence of experimental conditions. *Makromol. Chem.* **1992**, *193* (1), 1−9.
(36) Sharma, S.; Shyam Kumar, C. N.; Korvink, J. G.; Kubel, C. Evolution of glassy carbon microstructure: in situ transmission electron microscopy of the pyrolysis process. *Sci. Rep.* **2018**, *8* (1), 1−12.
(37) Carbon. In *Comprehensive Inorganic Chemistry II from Elements to Applications*; Poeppelmeier, K., Reedijk, J., Eds.; Elsevier, 2013; Chapter 7, pp 323−369.
(38) Thompson, A. P. LAMMPS - a flexible simulation tool for particle-based materials modeling at the atomic, meso, and continuum scales. *Comput. Phys. Commun.* **2022**, *271* (2022), 108−171.
(39) Aktulga, H. M.; Fogarty, J. C.; Pandit, S. A.; Grama, A. Y. Parallel reactive molecular dynamics: numerical methods and algorithmic techniques. *Parallel Computing* **2012**, *38* (4−5), 245−259.
(40) Senftle, T. P.; Hong, S.; Islam, M. M.; Kylasa, S. B.; Zheng, Y.; Shin, Y. K.; Junkermeier, C.; Engel-Herbert, R.; Janik, M. J.; Aktulga, H. M.; Verstraelen, T.; Grama, A.; van Duin, A. C. T. The ReaxFF reactive force-field: development, applications and future directions. *npj Computational Materials* **2016**, *2* (1), 1−14.
(41) Zhang, W.; van Duin, A. C. T. Improvement of the ReaxFF description for functionalized hydrocarbon/water weak interactions in the condensed phase. *J. Phys. Chem. B* **2018**, *122* (14), 4083−4092.
(42) Vashisth, A.; Ashraf, C.; Zhang, W.; Bakis, C. E.; van Duin, A. C. T. Accelerated ReaxFF simulations for describing the reactive cross-linking of polymers. *J. Phys. Chem. A* **2018**, *122* (32), 6633−6642.
(43) Stukowski, A. Visualization and analysis of atomistic simulation data with OVITO−the open visualization tool. *Modell. Simul. Mater. Sci. Eng.* **2010**, *18* (1), 015012.
(44) National center for biotechnology information. PubChem compound summary for CID 7361, furfuryl alcohol.https://pubchem.ncbi.nlm.nih.gov/compound/Furfuryl-alcohol#section=Density (accessed 2021).
(45) Furfuryl Alcohol. https://www.transfurans.be/building-construction (accessed 2020).
(46) Cowie, J. M. G. *Polymers: Chemistry and Physics of Modern Materials*; CRC Press, 2007.
(47) Odegard, G. M.; Jensen, B. D.; Gowtham, S.; Wu, J.; He, J.; Zhang, Z. Predicting mechanical response of crosslinked epoxy using ReaxFF. *Chem. Phys. Lett.* **2014**, *591* (2014), 175−178.
(48) Kowalik, M.; Ashraf, C.; Damirchi, B.; Akbarian, D.; Rajabpour, S.; van Duin, A. C. T. Atomistic scale analysis of the carbonization process for C/H/O/N-Based polymers with the ReaxFF reactive force field. *J. Phys. Chem. B* **2019**, *123* (25), 5357−5367.
(49) Srinivasan, S. G.; van Duin, A. C. T.; Ganesh, P. Development of a ReaxFF potential for carbon condensed phases and its application to the thermal fragmentation of a large fullerene. *J. Phys. Chem. A* **2015**, *119* (4), 571−580.
(50) Yoon, J.; Jang, Y.; Kim, K.; Kim, J.; Son, S.; Lee, Z. In situ tensile and fracture behavior of monolithic ultra-thin amorphous carbon in TEM. *Carbon* **2022**, *196* (2022), 236−242.
(51) Coleman, S. P.; Spearot, D. E.; Capolungo, L. Virtual diffraction analysis of Ni [0 1 0] symmetric tilt grain boundaries. *Modell. Simul. Mater. Sci. Eng.* **2013**, *21* (5), 055020.
(52) Li, C.; Strachan, A. Molecular dynamics predictions of thermal and mechanical properties of thermoset polymer EPON862/DETDA. *Polymer* **2011**, *52* (13), 2920−2928.
(53) Humphrey, W.; Dalke, A.; Schulten, K. VMD: visual molecular dynamics. *J. Mol. Graphics* **1996**, *14* (1), 33−38.

https://doi.org/10.1021/acsaenm.3c00360
ACS Appl. Eng. Mater. 2023, 1, 2555−2566